Inorganic Chemistry

ARTICLE

pubs.acs.org/IC

Insights into Dehydrogenative Coupling of Alcohols and Amines Catalyzed by a (PNN)−Ru(II) Hydride Complex: Unusual Metal−Ligand Cooperation

Guixiang Zeng and Shuhua Li*

Institute of Theoretical and Computational Chemistry, School of Chemistry and Chemical Engineering, Key Laboratory of Mesoscopic Chemistry of Ministry of Education, Nanjing University, Nanjing, 210093, P.R. China

Supporting Information

ABSTRACT: Density functional theory calculations were performed to elucidate the mechanism of dehydrogenative coupling of primary alcohols and amines mediated by a PNN−Ru(II) hydride complex (PNN = (2-(di-*tert*-butylphosphinomethyl)-6-(diethylaminomethyl)pyridine)). A plausible reaction pathway was proposed which contains three stages: (1) The alcohol dehydrogenation reaction to generate the aldehyde and H_2; (2) The aldehyde-amine condensation reaction to form the hemiaminal intermediate; (3) The dehydrogenation process of the hemiaminal intermediate to yield the final amide product with the liberation of H_2. The first and third stages occur via a similar pathway: (a) Proton transfer from the substrate to the PNN ligand; (b) Intramolecular rearrangement of the deprotonated substrate to form an anagostic complex; (c) Hydride transfer from the deprotonated substrate to the Ru center to yield the *trans*-dihydride intermediate and the aldehyde (or amide); (d) Benzylic proton migration from the PNN ligand to the metal center forming a dihydrogen complex and subsequent H_2 liberation to regenerate the catalyst. In all these steps, the metal−ligand cooperation plays an essential role. In proton transfer steps (a) and (d), the metal−ligand cooperation is achieved through the aromatization/dearomatization processes of the PNN ligand. While in steps (b) and (c), their collaboration are demonstrated by the formation of an anagostic interaction between Ru and the C−H bond and two ionic hydrogen bonds supported by the PNN ligand.

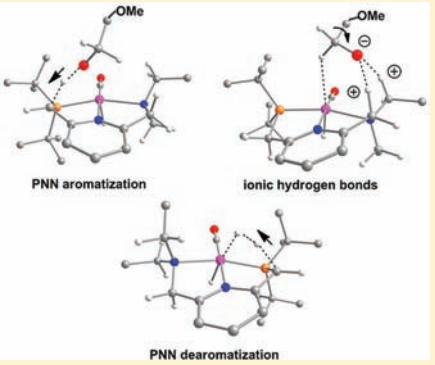

INTRODUCTION

In the past few decades, cooperative catalysis[1] based on new modes of metal−ligand cooperation has experienced an explosive progress for their powerful catalytic activity in the asymmetric synthesis,[2] C−H[3] and C−C[4] bonds activation, and so forth. Catalysts with pyridine-based PNN or PNP ligands[5] were found to exhibit remarkable catalytic reactivity in a number of novel and environmentally friendly reactions, such as reversible C−H and H−H bond activation,[6] the thermal H_2O decomposition,[7] dehydrogenation reactions which are coupled with unprecedented syntheses of amides, imines, esters, and ketones with the elimination of H_2.[8,9] For the first two types of reactions, their reaction mechanisms have been clarified theoretically.[10] Whereas the mechanism of dehydrogenation reactions are still unclear. Previously, a tentative mechanism has been suggested,[8,9] in which the PNN or PNP ligand changes its coordination from tri- to bidentate during the reaction so that the deprotonated substrate can coordinate with the metal center to form a precursor complex for the subsequent β−H elimination. However, the energetics of the reaction pathways in the proposed mechanism for dehydrogenation reactions has not been explored by computational studies.

In the present work, the dehydrogenative coupling of primary alcohols and amines mediated by the ruthenium hydride complex, (PNN)Ru(II)H(CO) (**1**) (PNN = (2-(di-*tert*-butylphosphinomethyl)-6-(diethylaminomethyl)pyridine)[9a] is investigated through density functional theory calculations. Specifically, the alcohol **2** (R^1=CH_2OMe) and the amine **9** (R^2=CH_2Ph) are chosen as substrates. This reaction produces the amide and H_2 with 99% yield (see eq 1).

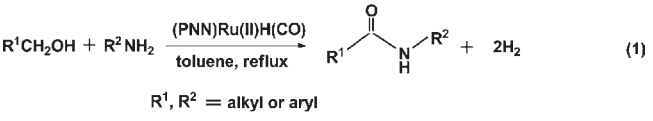

(1)

This type of reaction is of great importance because it provides an unprecedented efficient and atom economic method for the amide synthesis from very simple substrates.[11] On the other hand, it is closely related to the H_2 generation from alcohols, which is considered to be a promising way to produce H_2.[12] In this work, our purposes are to explore structural changes, free energy profiles for the reaction 1 as well as to elucidate the role of the metal−ligand cooperation in catalytic processes. Here, we propose an alternative pathway without ligand dissociation for the dehydrogenative coupling reaction, see Scheme 1.

Received: January 30, 2011
Published: September 26, 2011

Scheme 1. Our Proposed Pathways for the Dehydrogenation Reactions of the Alcohol (R = H) (2−7) and the Hemiaminal Intermediate (R = $NHCH_2Ph$) (11−15)

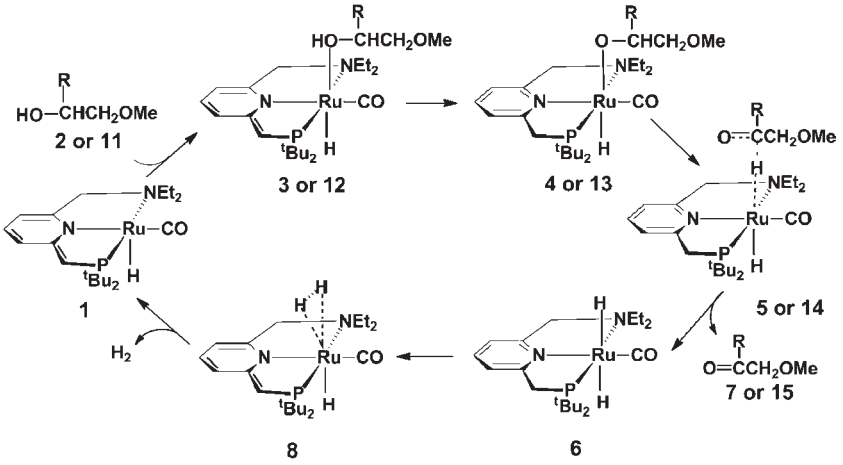

COMPUTATIONAL DETAILS

Geometry optimizations of all stationary points were performed using the B3LYP functional[13] implemented in the Gaussian03 program.[14a] The effective core potential LANL2DZ[15] was employed for the ruthenium (Ru) atom, and the LANL2DZ basis set supplemented with a set of 5p functions[16] and a set of f functions[17] were applied for the Ru atom. The 6-31G basis sets were used for eight methyl groups in the ruthenium hydride complex (the catalyst **1**), the $MeOCH_2$ group in the alcohol substrate ($MeOCH_2CH_2OH$) as well as the phenyl group and two hydrogen atoms on methylene in the amine compound ($PhCH_2NH_2$). For other atoms, the 6-311++G** basis sets were used. All stationary points were confirmed as minima or transition states through vibrational frequency calculations at the B3LYP level. In addition, transition states were verified by intrinsic reaction coordinate (IRC)[18] calculation. For each species, its gas−phase Gibbs free energy was computed at 383.78 K and 1.0 atm (the experimental conditions). We employed the polarizable−continuum model (PCM)[19] to treat the solvent effect with toluene as the solvent.

It is worthwhile mentioning how to calculate the Gibbs free energy (G_{sol}) in this work because it will be used exclusively to discuss reaction profiles in the next section. For a bimolecular process, such as the coordination of substrates **2** ($MeOCH_2CH_2OH$) or **9** ($PhCH_2NH_2$) with the catalyst **1**, the entropy change is significant. This fact should be taken into consideration in evaluating Gibbs free energy changes of these processes. For such cases, G_{sol} should be evaluated as follows:

$$\begin{aligned} G_{sol} &= H - T(S_r + S_v + S_t) \\ &= E^T + P\Delta V - T(S_r + S_v + S_t) \\ &= E_{sol} + E_{therm} - T(S_r + S_v + S_t) \end{aligned} \quad (2)$$

where ΔV is zero in solution, E_{therm} is the thermal correction from translational, vibrational, and rotational movements (calculated with B3LYP at its gas-phase optimized structure), S_r, S_v, and S_t are rotational, vibrational, and translational entropies, respectively. In general, the Sacker−Tetrode equation is used to evaluate the translational entropy S_t. However, in the solution phase, it cannot be directly applied to the evaluation of S_t, because it is significantly suppressed in solution.[20] Here, we evaluated the S_t with the method developed by Whitesides et al.[21] In eq 2, for each species, the total energy E_{sol}, the sum of the electronic energy and the free energy of solvation, was calculated using the M06−L functional[22] (implemented in Gaussian09 program[14b]) based on its gas−phase optimized structure.

To check the reliability of the M06−L single point calculation results, the activation energy barrier for the formation of the dihydrogen complex **8** (one of two rate-limiting steps) was also evaluated using MP4(SDQ)[23] single point calculations as well as well-behaved M06−L, M06,[24] M06−2x,[24] and LC−BLYP[25] functionals. In this procedure, all species involved were fully optimized using these functionals, respectively.

RESULTS AND DISCUSSION

In this section, we explored free energy profiles of the title reaction, which consists of the following three stages: (1) The dehydrogenation of the alcohol **2** to form the aldehyde **7** with the liberation of H_2, which is discussed in the first subsection. (2) The aldehyde−amine condensation reaction and its comparison with the aldol condensation reaction, presented in the next subsection. (3) The dehydrogenation of the hemiaminal intermediate affording the amide product, elucidated in the last subsection. These stages are in accordance with the tentative mechanism suggested previously.[8,9] The first and third stages proceed via a similar pathway (as shown in Scheme 1), with the complex **1** as the active catalyst. Since the triplet state surface is significantly higher than the singlet surface (see Supporting Information, Tables S1−S3 for details), we only discuss results on the singlet surface. Gibbs free energies in the solvent are exclusively used in discussions.

Activation free energy barrier (G_a) and reaction energy (ΔG) used in this text are defined as follows. If one intermediate is less stable in free energy than the initial reactants, G_a is defined as the free energy difference between the transition state and initial reactants. Otherwise, it is defined as the free energy difference between the transition state and the corresponding intermediate. ΔG is defined as the free energy difference between the products and the reactants for a given step.

Alcohol Dehydrogenation Reaction. Optimized geometries of all stationary points along the reaction pathway are displayed in Figures 1 and 2. The Gibbs free energy profile is presented in Figure 3.

In the catalyst (PNN)Ru(II)H(CO) **1**, N1−C1, C1−C2, and Ru−N1 distances are 1.394, 1.385, and 2.107 Å, respectively, showing that the PNN ligand has a dearomatized pyridine ring. In the alcohol substrate **2**, O1−H3 and O1−C3 distances are

dx.doi.org/10.1021/ic200205e |Inorg. Chem. 2011, 50, 10572–10580

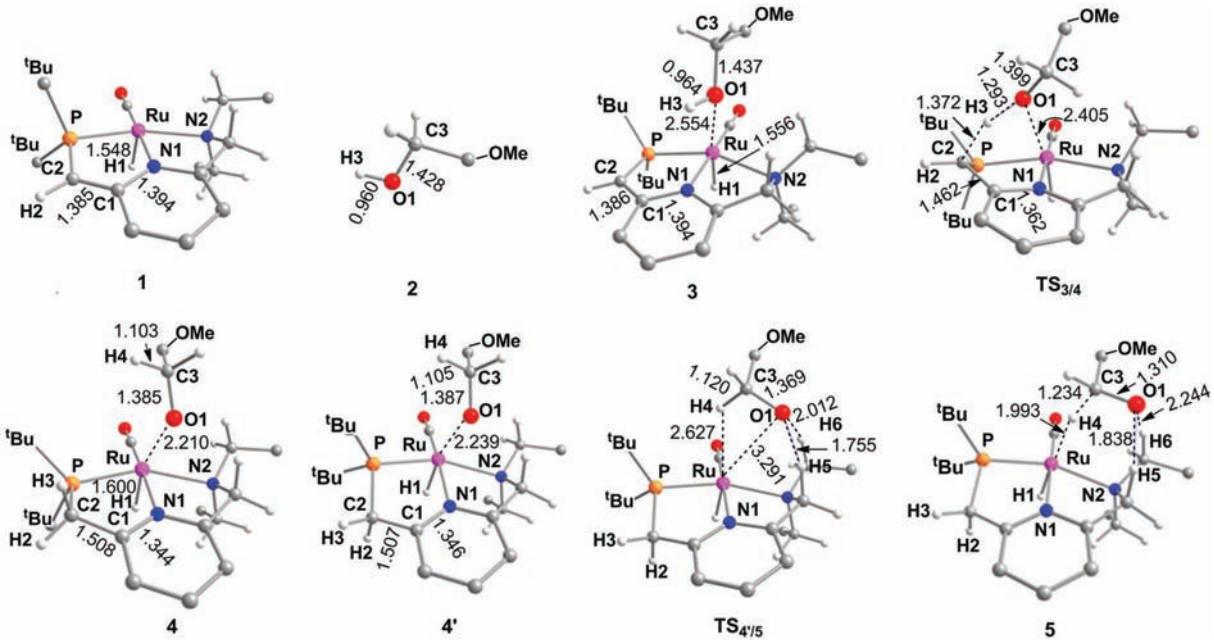

Figure 1. Optimized geometries of some species involved in alcohol (**2**) coordination, proton transfer, and intramolecular rearrangement steps along the alcohol dehydrogenation process. Hydrogen atoms except for those involved in the reaction are omitted for clarity. Distances are in Å.

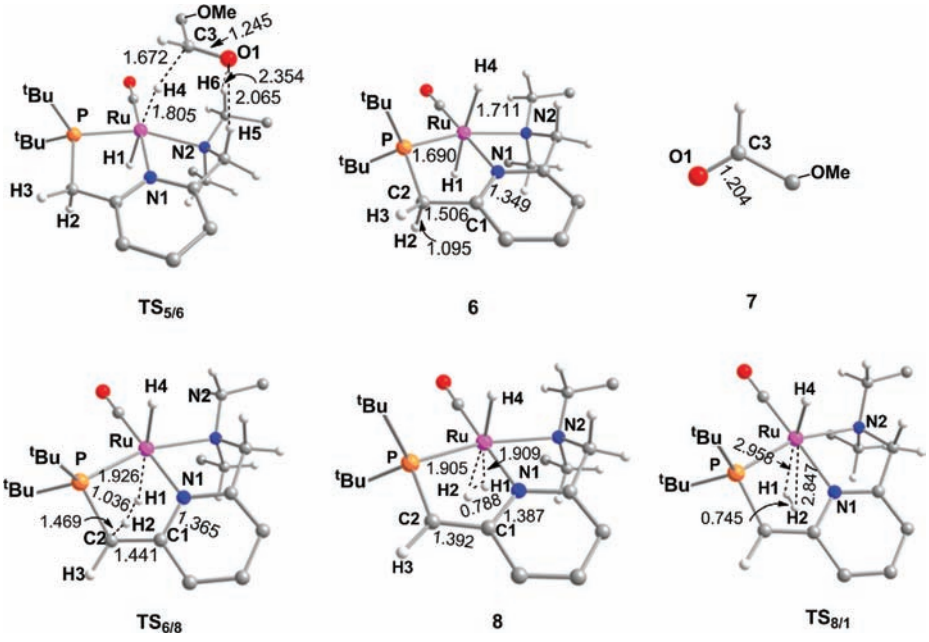

Figure 2. Optimized geometries of some species involved in the C−H bond activation and H_2 elimination steps along the alcohol dehydrogenation process. Hydrogen atoms except for those involved in the reaction are omitted for clarity. Distances are in Å.

0.960 and 1.428 Å, respectively. The reaction is initiated by the coordination of **2** with **1** leading to a precursor complex **3**. This addition step is moderately endothermic by 5.4 kcal/mol. In the complex **3**, the Ru−O1 distance is 2.554 Å, suggesting a weak Ru−O1 interaction. Because of the long Ru−O1 distance, O1−H3 and O1−C3 bond lengths of the alcohol moiety are only slightly elongated by 0.004 and 0.009 Å, respectively. On the other hand, geometrical parameters on the catalyst moiety also show little changes, that is, C1−C2 and Ru−N1 distances are elongated by 0.001 and 0.022 Å, respectively. These results indicate that the PNN ligand is not involved in this addition step. This conclusion is confirmed by the natural atomic change analysis, where the NBO charges on N1 (−0.49 *e*), C1 (0.21 *e*), and C2 (−0.79 *e*) in the complex **3** are almost the same as that in the complex **1** (−0.50 *e*, 0.21 *e*, and −0.79 *e* for N1, C1, and C2, respectively).

The next step is the proton (H3) transfer from the hydroxyl group of the alcohol moiety to the benzylic carbon (near the phosphorus atom) of the PNN ligand to form an intermediate **4**. In the corresponding transition state $\mathbf{TS_{3/4}}$, Ru−O1, O1−H3, and H3−C2 distances are 2.405, 1.293, and 1.372 Å, respectively.

dx.doi.org/10.1021/ic200205e |*Inorg. Chem.* 2011, 50, 10572–10580

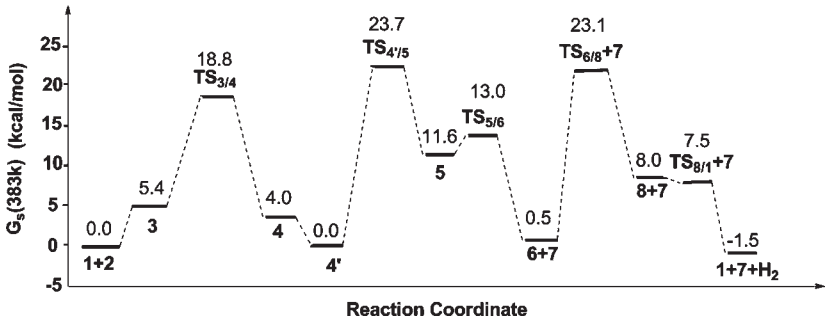

Figure 3. Gibbs free energy profile of the alcohol dehydrogenation reaction mediated by (PNN)Ru(II)H(CO) **1** in the solvent (toluene).

Table 1. Natural Atomic Charges on Oxygen and Hydrogen Atoms Involved in Ionic Hydrogen Bonds in Species $TS_{4'/5}$ and 5

species	O1	H5	H6
$TS_{4'/5}$	−0.97 *e*	0.33 *e*	0.26 *e*
5	−0.86 *e*	0.30 *e*	0.23 *e*

This step is exothermic by 1.4 kcal/mol, with G_a = 18.8 kcal/mol. In this process, the C1−C2 distance increases from 1.386 Å in **3**, 1.462 Å in $TS_{3/4}$ to 1.508 Å in **4**. At the same time, the C1−N1 distance decreases from 1.394 Å in **3** to 1.362 Å in $TS_{3/4}$, 1.344 Å in **4**. These structural changes indicate that the proton transfer process is concomitant with the aromatization process of the pyridine ring. On the other hand, the O1−Ru distance is significantly shortened by 0.344 Å in the species **4** relative to the species **3**, suggesting that a strong interaction between O1 and Ru is formed. Correspondingly, the O1−C3 distance also becomes shorter from 1.437 Å in **3**, 1.399 Å in $TS_{3/4}$ to 1.385 Å in **4**. It should be mentioned that in species **4** two five−membered rings formed by the PNN ligand and the Ru center are almost in the same plane. Species **4** can readily transform to a more stable species **4′** with two twisted five-membered rings, which lies below species **4** by 4.0 kcal/mol.

Next, an intramolecular rearrangement of the deprotonated alcohol moiety converts the species **4′** to an anagostic complex **5** via a transition state $TS_{4'/5}$. In $TS_{4'/5}$, the distances of Ru−H4, O1−H5, and O1−H6 are 2.627, 1.755, and 2.012 Å, respectively. The natural atomic charges on O1, H5, and H6 are −0.97*e*, 0.33*e*, and 0.26*e*, respectively. Thus, there are strong ionic hydrogen bonds[26] between O1 and two hydrogens, H5 (on the methylene spacer) and H6 (on the N-bonded ethyl group), respectively. Since the Ru−O1 bond (3.291 Å) is completely broken, the formation of these two ionic hydrogen bonds is critical for stabilizing $TS_{4'/5}$. In the anagostic complex **5**, C3−H4 and Ru···H4 distances are 1.234 and 1.993 Å, respectively, and the Ru−H4−C3 angle is 169°, indicating an anagostic interaction[27,28] between Ru and the C−H bond. The "anagostic" interaction means a M···H−C bonding interaction with long M···H distances and large M−H−C angles.[27c,28] Interestingly, the anagostic complex **5** is also found to be stabilized by two ionic hydrogen bonds, between O1 and H5 (1.838 Å), O1 and H6 (2.244 Å), respectively. The NBO charges on these atoms are listed in Table 1. In this step, the O1−C3 distance becomes further shorter from 1.387 in **4′** to 1.369 in $TS_{4'/5}$, and to 1.310 Å in the species **5**. Please note that the carbon atom C3 in **5** is actually in the normal valence state. On one hand, the O1−C3 bond length is between a typical C−O single bond (around 1.43 Å) and a typical C=O bond distance (about 1.20 Å). On the other hand, the C3−H4 bond (1.236 Å) is much activated as compared to a typical C−H bond (1.09 Å). Hence, the $[(MeOCH_2)(H)(R)C-O]^-$ moiety can be considered to be an alkoxide. This reaction step is endothermic by 11.6 kcal/mol with G_a = 23.7 kcal/mol.

In the next step, the hydride H4 transfers from the C3 atom of the deprotonated substrate to the Ru center via the transition state $TS_{5/6}$, generating the *trans*-dihydride complex **6** and the aldehyde **7**. In $TS_{5/6}$, C3−H4 and Ru−H4 distances are 1.672 and 1.805 Å, respectively, indicating that the C−H bond is already broken and the Ru−H bond is almost formed. The O1−C3 distance (1.245 Å) is close to that in the species **7** (1.204 Å), suggesting that the O1−C3 double bond is formed. This hydride transfer step is exothermic by 11.1 kcal/mol, with G_a = 13.0 kcal/mol. One should note that $TS_{5/6}$ is slightly higher than the intermediate **5** by only 1.4 kcal/mol, indicating a facile hydride transfer process.

In the *trans*-dihydride complex **6**, Ru−H1 and Ru−H4 distances are 1.690 and 1.711 Å, respectively. In the subsequent step, one of the benzylic hydrogens (next to the phosphorus atom) transfers to the metal center to form a dihydrogen complex **8** through the transition state $TS_{6/8}$. In $TS_{6/8}$, Ru−H1, H1−H2, and H2−C2 distances are 1.926, 1.036, and 1.469 Å, respectively. This step is endothermic by 7.5 kcal/mol, with an activation barrier of 23.1 kcal/mol. In the dihydrogen complex **8**, the H1−H2 distance (0.788 Å) is slightly longer than that in the free H_2 (0.745 Å). During this reaction step, the C1−C2 distance decreases from 1.506 Å in **6**, to 1.441 Å in $TS_{6/8}$, and to 1.392 Å in **8**. Simultaneously, the C1−N1 distance increases from 1.349 Å in **6**, 1.365 Å in $TS_{6/8}$ to 1.387 Å in **8**. These structural changes indicate that the pyridine ring is dearomatized in this proton transfer process.

Finally, the catalyst **1** is regenerated through the H_2 elimination from the dihydrogen complex **8**. In this reaction step, Ru−H1 and Ru−H2 distances considerably increase from 1.909 and 1.905 Å in **8** to 2.958 and 2.847 Å in $TS_{8/1}$, respectively. This step involves an activation barrier of 7.5 kcal/mol with the exothermicity of 9.5 kcal/mol. It should be pointed out that the transition state $TS_{8/1}$ is slightly lower (by 0.5 kcal/mol) in free energy than the dihydrogen complex **8**. However, $TS_{8/1}$ is higher than **8** by 3.4 kcal/mol in electronic energy. The nearly equivalent thermodynamic stability of $TS_{8/1}$ and **8** may result from the harmonic approximation in computing the vibrational frequencies.

To evaluate the reliability of G_a and ΔG values calculated with M06−L single point calculations, we re-evaluate the values of G_a and ΔG for the formation step of the dihydrogen complex **8**

dx.doi.org/10.1021/ic200205e |*Inorg. Chem.* 2011, 50, 10572–10580

using the MP4(SDQ) method and density functional theory with M06−L, M06, M06−2x, and LC−BLYP functionals. With the same basis set, we have optimized the geometries of related species using these functionals, collected in Supporting Information, Figures S1−S2. The calculated G_a and ΔG values are tabulated in Table 2. As shown in Table 2, if the MP4(SDQ) method is used, G_a and ΔG are 24.3 and −1.8 kcal/mol, respectively. For M06−family functionals, M06−L (24.0/−1.9 kcal/mol), M06 (26.5/−1.2 kcal/mol) as well as single point calculations using M06−L (22.6/−1.5 kcal/mol, based on B3LYP-optimized geometries) provide similar results as the MP4(SDQ) method. However, M06−2x (33.8/1.4) and LC−BLYP (33.5/5.0) functionals considerably overestimate both G_a and ΔG. Thus, M06−L single point calculations based on B3LYP-optimized geometries provide reasonable results.

Table 2. Gibbs Free Energy Barriers (G_a)[a] and Reaction Energies (ΔG)[b] Calculated by Density Functional Theory with Various Functionals and the MP4(SDQ) Method

method	G_a (kcal/mol)	ΔG (kcal/mol)
MP4(SDQ)[c]	24.3	−1.8
M06−L	24.0	−1.9
M06−L-sp[c]	22.6	−1.5
M06	26.5	−1.2
M06−2x	33.8	1.4
LC−BLYP	33.5	5.0

[a] G_a is defined as the Gibbs free energy difference between ($TS_{6/8}$ +7) and (**1**+**2**). [b] ΔG is defined as the Gibbs free energy difference between (7 + H_2) and **2**. [c] Single point calculation results based on the B3LYP−optimized structures.

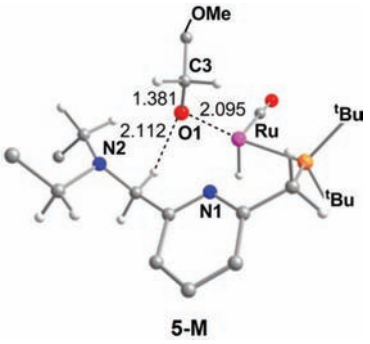

Figure 4. Optimized structure of **5**−**M**. Hydrogen atoms except for those involved in the reaction are omitted for clarity. Distances are in Å.

To summarize, our calculations show that the alcohol dehydrogenation reaction includes the following steps: (1) The proton migration from the hydroxyl group of the alcohol moiety to the benzylic carbon of the PNN ligand; (2) Intramolecular rearrangement leading to an anagostic complex **5**; (3) The hydride transfer from the deprotonated substrate to the Ru center to generate the intermediate aldehyde **7** and a dihydride complex **6**; (4) Starting from the complex **6**, one benzylic proton transfers from the PNN ligand to the metal center to form a dihydrogen complex **8** and then H_2 eliminates to recover the catalyst **1**. In all these catalytic processes, the cooperation between the metal center and the PNN ligand plays a very important role. In steps (1) and (4), they cooperate with each other through the aromatization/dearomatization processes of the PNN ligand. In steps (2) and (3), the deprotonated substrate is stabilized by its coordination to the metal center and two ionic hydrogen bonds supported by two hydrogen atoms on the PNN ligand. The latter metal−ligand cooperation mode is first pointed out here.

In the mechanism proposed previously,[8,9] a key intermediate (denoted as **5**−**M**) is expected to be generated through the intramolecule rearrangement of the species **4**′ with the Ru−N2 bond breaking. The fully optimized structure of **5**−**M** is shown in Figure 4. This species is higher than the related species **5** (on the pathway described above) by about 2.2 kcal/mol, and is higher than the reactants (**1**+**2**) by 13.8 kcal/mol. For the subsequent

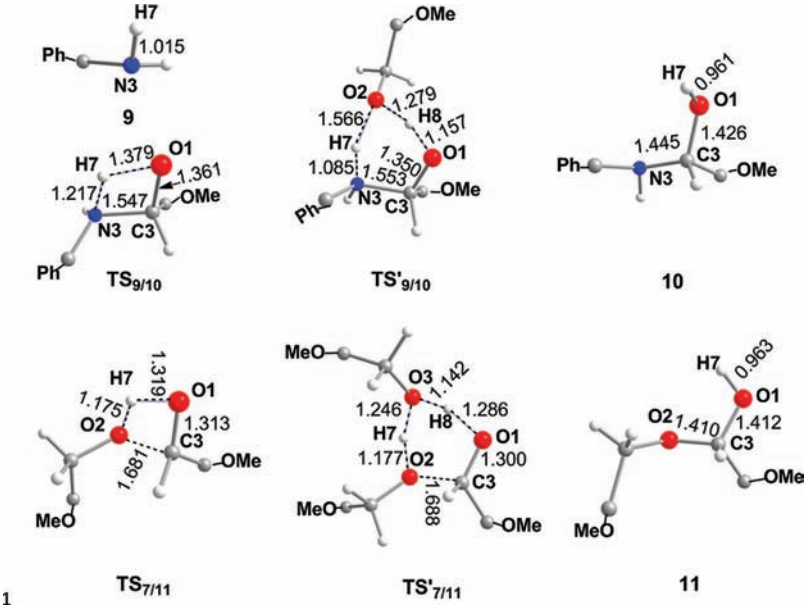

Figure 5. Optimized geometries of some stationary points involved in uncatalyzed aldehyde−amine and aldol condensation reactions. Hydrogen atoms except for those involved in the reaction are omitted for clarity. Distances are in Å. In $TS'_{9/10}$ and $TS'_{7/11}$, an alcohol molecule is used as a bridge, respectively.

dx.doi.org/10.1021/ic200205e |*Inorg. Chem.* 2011, 50, 10572–10580

β−H elimination step in the previously proposed mechanism (following the formation of **5**−**M**), we could not locate the corresponding transition state. However, since $\mathbf{TS}_{5/6}$ is above the reactants (**1**+**2**) by only 13.0 kcal/mol, and the transition state of the β−H elimination step (if it exists) must lie higher than the intermediate **5**−**M**, one can deduce that the pathway we suggested above for the dehydrogenation process is preferred.

Aldehyde−Amine and Aldol Condensation Reactions. In this reaction stage, the aldehyde **7** condenses with the amine **9** (or the alcohol **2**) to form the hemiaminal intermediate **10** (or the hemiacetal intermediate **11**). Note that, the catalyst (PNN)-Ru(II)H(CO) does not participate in these two condensation reactions. Optimized geometries of all species involved in condensation reactions are shown in Figure 5 and the free energy profile is displayed in Figure 6.

In the aldehyde−amine condensation reaction, the hemiaminal intermediate **10** is formed through the migration of the proton H7 from the amine **9** to the aldehyde **7**, which lies higher than the reactants (**7** + **9**) by 8.4 kcal/mol, as shown in Figure 6a. In the transition state $\mathbf{TS}_{9/10}$, H7 directly transfers from N3 to O1. N3−H7, H7−O1, O1−C3, and C3−N3 distances are 1.217, 1.379, 1.361, and 1.547 Å, respectively. The activation energy barrier (G_a) is estimated to be 37.7 kcal/mol. This large G_a may be ascribed to the significant tension of the four−membered ring formed in the transition state. In fact, this proton transfer process can be facilitated by using an alcohol molecule as a bridge. The corresponding transition state, $\mathbf{TS'}_{9/10}$, was successfully located. In $\mathbf{TS'}_{9/10}$, N3, H7, O2, H8, O1, and C3 form a six−membered ring, so that the ring tension is considerably reduced. As a result, the G_a decreases from 37.7 ($\mathbf{TS}_{9/10}$) to 28.8 kcal/mol ($\mathbf{TS'}_{9/10}$).

In the aldol condensation reaction, the hemiacetal **11** is formed through the proton transfer from the alcohol **2** to the aldehyde **7**, which is 11.6 kcal/mol above reactants (**7** + **2**), as shown in Figure 6b. The direct proton transfer pathway via the transition state $\mathbf{TS}_{7/11}$ involves a relatively high G_a, 44.3 kcal/mol. Similar to the aldehyde−amine reaction, the proton transfer with an alcohol molecule as a bridge (via the transition state of $\mathbf{TS'}_{7/11}$) can reduce G_a to 39.5 kcal/mol.

In principle, the hemiacetal intermediate **11** can be dehydrogenated by the catalyst **1** to form an ester, and then the reaction of this ester with the amine may also produce the amide product. Although some amides have been successfully synthesized from esters and amines,[29] reactions between esters and benzylamines (like the amine **9**) were ruled out by related experiments.[9a]

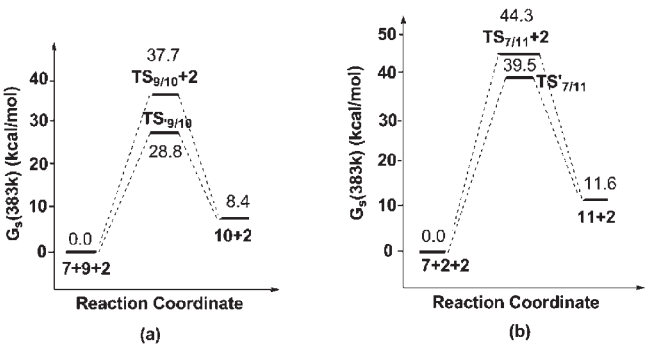

Figure 6. (a) Gibbs free energy profile of the aldehyde−amine condensation reaction; (b) Gibbs free energy profile of the aldol condensation reaction.

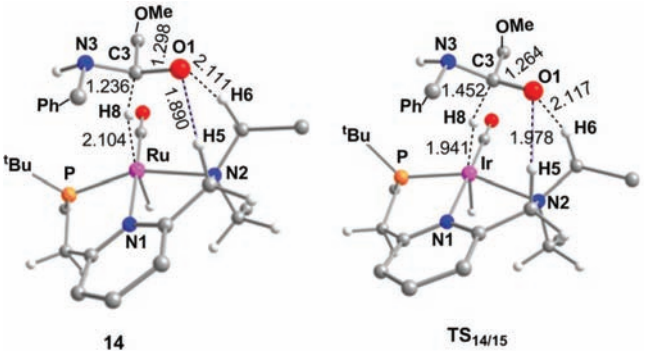

Figure 8. Optimized structures for **14** and $\mathbf{TS}_{14/15}$ involved in the hemiaminal dehydrogenation reaction obtained with the M06−2x functional. Hydrogen atoms except for those involved in the reaction are omitted for clarity. Distances are in Å.

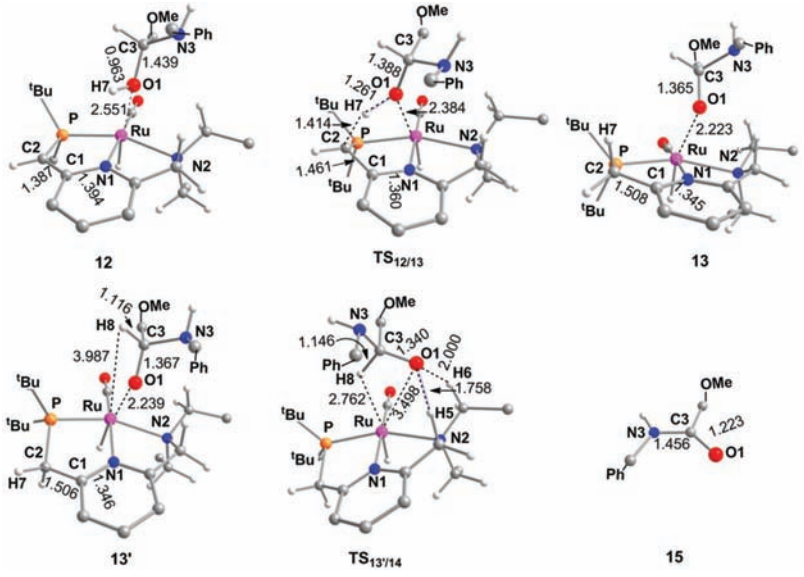

Figure 7. Optimized geometries of some species involved in the hemiaminal dehydrogenation reaction. Hydrogen atoms except for those involved in the reaction are omitted for clarity. Distances are in Å.

dx.doi.org/10.1021/ic200205e |*Inorg. Chem.* 2011, 50, 10572–10580

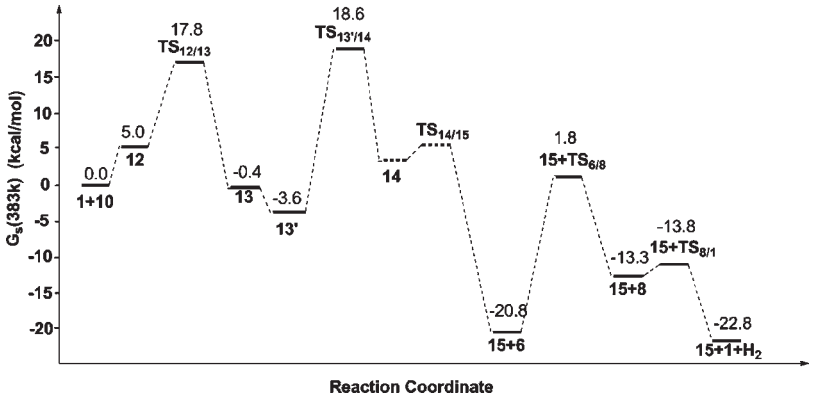

Figure 9. Free energy profile of the hemiaminal dehydrogenation mediated by **1** in the solvent. **14** and $\mathbf{TS_{14/15}}$ are located with the M06−2x functional (see the text).

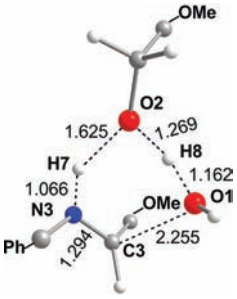

Figure 10. Transition state $\mathbf{TS-H_2O}$ for the dehydration of the hemiaminal **10**. An alcohol molecule is used as a bridge. Hydrogen atoms except for those involved in the reaction are omitted for clarity. Distances are in Å.

In summary, the aldehyde−amine condensation reaction (G_a/ΔG: 28.8/8.4 kcal/mol) is more favorable than the aldol condensation reaction (G_a/ΔG: 39.5/11.6 kcal/mol) both thermodynamically and kinetically. Thus, the formation of the hemiaminal species **10** is preferred for the subsequent reactions. In the aldehyde−amine condensation, the alcohol bridged proton transfer process is more favorable.

Hemiaminal Dehydrogenation Reaction. The dehydrogenation of the hemiaminal species **10** proceeds via a similar pathway to the dehydrogenation of the alcohol **2** (Scheme 1), as described above. Optimized geometries of all stationary points along the reaction pathway are provided in Figures 7 and 8. The free energy profile is presented in Figure 9. In this reaction stage, species **12**, **13**, **14′**, and **14** in Figure 7 are structural analogues of **3**, **4**, **4′**, and **5** in Figure 1, respectively.

First, the precursor complex **12** is formed through the coordination of the hemiaminal compound **10** with the catalyst **1**, which is less stable by 5.0 kcal/mol than reactants (**1**+**10**). Next, the PNN pincer ligand is aromatized by the proton migration from the hydroxyl group of the hemiaminal moiety to the benzylic arm (near the phosphorus atom) of the PNN ligand through $\mathbf{TS_{12/13}}$. In $\mathbf{TS_{12/13}}$, Ru−O1, O1−H7, and H7−C2 distances are 2.384, 1.261, and 1.414 Å, respectively. The values of G_a and ΔG for this step are 17.8 and −5.4 kcal/mol, respectively. In the complex **13**, like the complex **4**, the PNN ligand and the Ru center form two five-membered rings, which are almost in the same plane. By twisting these two five-membered rings, species **13** can readily transform to a more stable species **13′**, which is below **13** by 3.2 kcal/mol.

Similar to the transformation from species **4′** to the anagostic complex **5**, the intramolecular rearrangement of the species **13′** to form an anagostic complex **14** is likely to occur. This step takes place through $\mathbf{TS_{13'/14}}$. Like in $\mathbf{TS_{4'/5}}$, $\mathbf{TS_{13'/14}}$ is also stabilized by two strong ionic hydrogen bonds, between O1−H5 (1.758 Å) and O1−H6 (2.000 Å), in which the natural atomic charges on O1, H5, and H6 are −0.86*e*, 0.30*e*, and 0.23*e*, respectively. This step involves an activation barrier of 22.2 kcal/mol. In this step, the Ru−O1 bond is broken, and in the meantime, the C3−H8 bond approaches to the Ru center (the Ru−H8 distance is 2.762 Å in $\mathbf{TS_{13'/14}}$). However, the anagostic complex **14** (structural analogue of **5**) and its subsequent hydride transfer transition state $\mathbf{TS_{14/15}}$ along this pathway could not be located using the B3LYP functional. This is probably because the potential energy surface near the species **14** (and $\mathbf{TS_{14/15}}$) is very flat so that the B3LYP functional are not accurate enough for quantitative descriptions of this region. Our minimum structure optimizations starting from the transition state $\mathbf{TS_{13'/14}}$ always lead to the product amide **15** and the dihydride complex **6**. Nevertheless, structures of **14** and $\mathbf{TS_{14/15}}$ can be successfully located using the M06−2x functional.[29] Optimized structures of these two species are shown in Figure 8.

In the M06−2x−optimized structure of **14**, C3−H8 and Ru−H8 distances are 1.236 and 2.104 Å, respectively, and the Ru−H8−C3 angle is 162°, indicating an anagostic interaction between Ru and the C−H bond. M06−2x calculations show that the hydride transfer transition state, $\mathbf{TS_{14/15}}$, is only 1.0 kcal/mol above the anagostic complex **14**. These results confirm the flat potential energy surface around **14** or $\mathbf{TS_{14/15}}$. The products of this hydride transfer step are the *trans*-dihydride species **6** and the amide species **15**, in which O1−C3 and C3−N2 bond lengths are 1.223 and 1.456 Å, respectively. After the amide (**15**) is generated, the subsequent H_2 elimination from the *trans*-dihydride complex **6** to recover the catalyst **1** follows the same pathway as described in the subsection 3.1.

For the heminaminal species **10**, it is also possible to undergo the dehydration reaction to produce the imine. Here, we have also investigated this possibility. The transition state for the H_2O elimination step is presented in Figure 10. In our calculations, an alcohol molecule was used as a bridge to facilitate the proton migration from the amine group to the hydroxyl group to form H_2O. The activation barrier for this step is calculated to be 31.4 kcal/mol, which is much higher than that of each step in the hemiaminal dehydrogenation reaction (as shown in Figure 9).

Thus, the hemiaminal compound **10** prefers to undergo the dehydrogenation reaction rather than the dehydration reaction.

In summary, the pathway of the dehydrogenation reaction of the hemiaminal **10** is similar to that of the alcohol dehydrogenation reaction. As shown in Figure 9, the overall reaction is exothermic by 22.8 kcal/mol. The intramolecular rearrangement and the formation of the dihydrogen complex **8** need comparable activation barriers (22.2 and 22.6 kcal/mol, respectively), and thus both are the rate−limiting steps in the dehydrogenation reaction of the hemiaminal **10**.

CONCLUSION

We have performed a theoretical investigation on the reaction mechanism of the dehydrogenative coupling of primary alcohols and amines mediated by the catalyst (PNN)Ru(II)H(CO) **1**. Our proposed pathway for the whole catalytic process includes the following three stages: (1) the catalyzed dehydrogenation of the alcohol **2** to form the aldehyde intermediate **7**; (2) the aldehyde−amine condensation reaction without the participation of the catalyst to form the hemiaminal intermediate **10**; (3) the catalyzed dehydrogenation of the hemiaminal intermediate to yield the amide **15**. The first and third stages proceed via a similar pathway (Scheme 1), consisting of four steps: (a) Proton transfer from the hydroxyl group of the substrate to the benzylic carbon of the PNN ligand; (b) Intramolecular rearrangement of the deprotonated substrate to form an anagostic intermediate; (c) Hydride transfer from the deprotonated substrate to the Ru center to generate the product aldehyde (or amide) and the *trans*-dihydride intermediate; (d) The benzylic hydrogen transfer from the PNN ligand to the metal center to form a dihydrogen complex and then H_2 is eliminated to recover the catalyst **1**. Since steps (b) and (d) have comparable free energy barriers, both steps should be considered as rate-determining steps. In all reaction steps described above, the metal center and the PNN ligand were found to cooperate with each other in a synergistic manner. In proton transfer steps (a) and (d), the metal−ligand cooperation is achieved through the aromatization/dearomatization processes of the PNN ligand. In steps (b) and (c), the deprotonated substrate is stabilized by its coordination to the metal center and two ionic hydrogen bonds supported by two hydrogen atoms on the PNN ligand. The latter metal−ligand cooperation is rarely known before.

In the second stage, the aldehyde−amine condensation reaction yielding the hemiaminal intermediate **10** is found to be more favorable than the aldol condensation reaction. In the condensation reaction, one alcohol molecule is most likely to participate as a bridge for the proton transfer process. Our calculations also show that the hemiaminal intermediate **10** prefers to undergo the dehydrogenation reaction to produce the amide rather than the dehydration reaction to produce the imine. This result is consistent with the experimental facts that the amide product is obtained in 99% yield for the title reaction.

In summary, our theoretical investigations have suggested a plausible reaction mechanism for the dehydrogenative coupling of alcohols and amines mediated by the PNN-based catalyst **1**. A new metal−ligand cooperation mode is proposed from the present study. The information provided in this work is also valuable for understanding the related catalytic processes mediated by PNN−Ru(II) or PNP−Ru(II) hydride complexes.

ASSOCIATED CONTENT

Supporting Information. Single-point M06−L electronic energies in toluene solvent (E_{sol}), B3LYP-calculated zero-point energy (ZPE), entropies and thermal correction energies (E_{therm}) of all stationary points located in this work. This material is available free of charge via the Internet at http://pubs.acs.org.

AUTHOR INFORMATION

Corresponding Author
*E-mail: shuhua@nju.edu.cn.

ACKNOWLEDGMENT

Prof. Shigeyoshi Sakaki and Dr. Atsushi Ishikawa are gratefully acknowledged for helpful discussions. This work was supported by the National Natural Science Foundation of China (Grants 21073086 and 20833003), and the National Basic Research Program (Grant 2011CB808501). Part of the calculations were performed at the High Performance Computing Center of Nanjing University and the Shanghai Supercomputer Center (SSC, China).

REFERENCES

(1) (a) Morris, R. H. *Chem. Soc. Rev.* **2009**, *38*, 2282. (b) Ohkuma, T.; Utsumi, N.; Tsutsumi, K.; Murata, K.; Sandoval, C.; Noyori, R. *J. Am. Chem. Soc.* **2006**, *128*, 8724. (c) Noyori, R.; Yamakawa, M.; Hashiguchi, S. *J. Org. Chem.* **2001**, *66*, 7931. (d) Noyori, R.; Ohkuma, T. *Angew. Chem., Int. Ed.* **2001**, *40*, 40. (e) Noyori, R.; Hashiguchi, S. *Acc. Chem. Res.* **1997**, *30*, 97.

(2) (a) Ma, J. A.; Cahard, D. *Angew. Chem., Int. Ed.* **2004**, *43*, 4566. (b) Kanai, M.; Kato, N.; Ichikawa, E.; Shibasaki, M. *Synlett* **2005**, 1491. (c) Paull, D. H.; Abraham, C. J.; Scerba, M. T.; Alden-Danforth, E.; Lectka, T. *Acc. Chem. Res.* **2008**, *41*, 655 and references cited therein.

(3) (a) Ritleng, V.; Sirlin, C.; Pfeffer, M. *Chem. Rev.* **2002**, *102*, 1731. (b) Jun, C. H.; Moon, C. W.; Lee, D. Y. *Chem.—Eur. J.* **2002**, *8*, 2422. (c) Godula, K.; Sames, D. *Science* **2006**, *312*, 67.

(4) (a) Jun, C. H. *Chem. Soc. Rev.* **2004**, *33*, 610. (b) Alberico, D.; Scott, M. E.; Lautens, M. *Chem. Rev.* **2007**, *107*, 174.

(5) (a) van der Vlugt, J. I.; Reek, J. N. H. *Angew. Chem., Int. Ed.* **2009**, *48*, 8832. (b) Taylor, R. A.; Law, D. J.; Sunley, G. J.; White, A. J. P.; Britovsek, G. J. P. *Angew. Chem., Int. Ed.* **2009**, *48*, 8178. (c) Albrecht, M.; van Koten, G. *Angew. Chem., Int. Ed.* **2001**, *40*, 3750. (d) van der Boom, M. E.; Milstein, D. *Chem. Rev.* **2003**, *103*, 1759. (e) Jensen, C. M. *Chem. Commun.* **1999**, 2443. (f) Vigalok, A.; Milstein, D. *Acc. Chem. Res.* **2001**, *34*, 798. (g) Milstein, D. *Pure Appl. Chem.* **2003**, *75*, 445. (h) Milstein, D. *Top. Catal.* **2010**, *53*, 915. (i) van der Vlugt, J. I.; Pidko, E. A.; Vogt, D.; Lutz, M.; Spek, A. L. *Inorg. Chem.* **2009**, *48*, 7513.

(6) (a) Zhang, J.; Leitus, G.; Ben-David, Y.; Milstein, D. *J. Am. Chem. Soc.* **2006**, *128*, 15930. (b) Gunanathan, C.; Gnanaprakasam, B.; Iron, M. A.; Shimon, L. J. W.; Milstein, D. *J. Am. Chem. Soc.* **2010**, *132*, 14763.

(7) (a) Kohl, S. W.; Weiner, L.; Schwartsburd, L.; Konstantinovski, L.; Shimon, L. J. W.; Ben-David, Y.; Iron, M. A.; Milstein, D. *Science* **2009**, *324*, 74. (b) Hetterscheid, D. G. H. J.; Van der Vlugt, I.; De Bruin, B.; Reek, J. N. H. *Angew. Chem., Int. Ed.* **2009**, *48*, 8178.

(8) (a) Zhang, J.; Gandelman, M.; Shimon, L. J. W.; Rozenberg, H.; Milstein, D. *Organometallics* **2004**, *23*, 4026. (b) Zhang, J.; Leitus, G.; Ben-David, Y.; Milstein, D. *J. Am. Chem. Soc.* **2005**, *127*, 12429. (c) Zhang, J.; Leitus, G.; Ben-David, Y.; Milstein, D. *Angew. Chem., Int. Ed.* **2006**, *45*, 1113. (d) Balaraman, E.; Gnanaprakasam, B.; Shimon, L. J. W.; Milstein, D. *J. Am. Chem. Soc.* **2010**, *132*, 16756.

(9) (a) Gunanathan, C.; Ben-David, Y.; Milstein, D. *Science* **2007**, *317*, 790. (b) Gnanaprakasam, B.; Zhang, J.; Milstein, D. *Angew. Chem., Int. Ed.* **2010**, *49*, 1468. (c) Poverenov, E.; Gandelman, M.; Shimon, L. J. W.; Rozenberg, H.; Ben-David, Y.; Milstein, D. *Chem.—Eur. J.* **2004**, *10*, 4673.

(10) (a) Li, J.; Shiota, Y.; Yoshizawa, K. *J. Am. Chem. Soc.* **2009**, *131*, 13584. (b) Yang, X.; Hall, M. B. *J. Am. Chem. Soc.* **2010**, *132*, 120. (c) Zeng, G.; Guo, Y.; Li, S. *Inorg. Chem.* **2009**, *48*, 10257. (d) Iron, M. A.; Ben-Ari, E.; Cohen, R.; Milstein, D. *Dalton Trans.* **2009**, 9433.

(11) (a) Keense, F. R. *Coord. Chem. Rev.* **1999**, *187*, I21. (b) Martinelli, J. R.; Clark, T. P.; Watson, D. A.; Munday, R. H.; Buchwald, S. L. *Angew. Chem., Int. Ed.* **2007**, *46*, 8460. (c) Chan, W. K.; Ho, C.-M.; Wong, M. K.; Che, C. M. *J. Am. Chem. Soc.* **2006**, *128*, 14796.

(12) (a) Friendrich, A.; Schneider, S. *ChemCatChem* **2009**, *1*, 72. (b) Johnson, T. C.; David J. Morris, D. J.; Wills, M. *Chem. Soc. Rev.* **2010**, *39*, 81. (c) Junge, H.; Loges, B.; Beller, M. *Chem. Commun.* **2007**, 522. (d) Sieffert, N.; Bühl, M. *J. Am. Chem. Soc.* **2010**, *132*, 8056.

(13) (a) Becke, A. D. *J. Chem. Phys.* **1993**, *98*, 5648. (b) Lee, C.; Yang, W.; Parr, R. G. *Phys. Rev. B.* **1988**, *37*, 785.

(14) (a) Frisch, M. J.; et al. *Gaussian 03*, revision D.01; Gaussian Inc.: Wallingford, CT, 2004. (b) Frisch, M. J.; et al. *Gaussian 09*, revision A.02; Gaussian Inc.: Wallingford, CT, 2009.

(15) Hay, P. J.; Wadt, W. R. *J. Chem. Phys.* **1985**, *82*, 299.

(16) Couty, M.; Hall, M. B. *J. Comput. Chem.* **1996**, *17*, 1359.

(17) Ehlers, A. W.; Böhme, M.; Dapprich, S.; Gobbi, A.; Höllwarth, A.; Jonas, V.; Köhler, K. F.; Stegmann, R.; Veldkamp, A.; Frenking, G. *Chem. Phys. Lett.* **1993**, *208*, 111.

(18) Gonzalez, C.; Schlegel, H. B. *J. Chem. Phys.* **1989**, *90*, 2154.

(19) Tomasi, J.; Persico, M. *Chem. Rev.* **1994**, *94*, 2027.

(20) (a) Sakaki, S.; Ohnishi, Y.; Sato, H. *Chem. Rec.* **2010**, *10*, 29. (b) Ishikawa, A.; Nakao, Y.; Sato, H.; Sakaki, S. *Dalton Trans.* **2010**, *39*, 3279. (c) Ishikawa, A.; Nakao, Y.; Sato, H.; Sakaki, S. *Inorg. Chem.* **2009**, *48*, 8154. (d) Ohnishi, Y.; Nakao, Y.; Sato, H.; Hiyama, T.; Sakaki, S. *Organometallics* **2009**, *28*, 2583.

(21) Mammen, M.; Shakhnovich, E. I.; Deutch, J. M.; Whitesides, G. M. *J. Org. Chem.* **1998**, *63*, 3821.

(22) Zhao, Y.; Truhlar, D. G. *J. Chem. Phys.* **2006**, *125*, 194101.

(23) (a) Pople, J. A. *Int. J. Quantum Chem.* **1978**, *14*, 91. (b) Raghavachari, K.; Frisch, M. J.; Pople, J. A. *Chem. Phys. Lett.* **1980**, *72*, 4244.

(24) Zhao, Y.; Truhlar, D. *Theor. Chem. Acc.* **2008**, *120*, 215.

(25) Iikura, H.; Tsuneda, T.; Yanai, T.; Hirao, K. *J. Chem. Phys.* **2001**, *115*, 3540.

(26) Mautner, M. *Chem. Rev.* **2005**, *105*, 213 and references cited therein.

(27) (a) Brammer, L.; Charnock, J. M.; Goggin, P. L.; Goodfellow, R. J.; Koetzle, T. F.; Orpen, A. G. *J. Chem. Soc., Chem. Commun.* **1987**, 443. (b) Brammer, L.; Charnock, J. M.; Goggin, P. L.; Goodfellow, R. J.; Orpen, A. G.; Koetzle, I. F. *J. Chem. Soc., Dalton Trans.* **1991**, 1789. (c) Braga, D.; Grepioni, F.; Tedesco, E.; Biradha, K.; Desiraju, G. R. *Organometallics* **1997**, *16*, 1846.

(28) (a) Calhorda, M. J. *Chem. Commun.* **2000**, 80. (b) Brookhart, M.; Green, M. L. H.; Parkin, G. *Proc. Nat. Acad. Sci.* **2007**, *104*, 6908.

(29) Gnanaprakasam, B.; Milstein, D. *J. Am. Chem. Soc.* **2011**, *133*, 1682.